An Unbiased Multiparameter Algorithm of Retrieving Sea Surface Height Using Coastal GNSS Reflectometry

Feng Wang, Zhichao Xu, Dongkai Yang, GuoDong Zhang, Jin Xing, Zhejia Shi, Bo Zhang, and Lei Yang

***Abstract*—Due to the diffuse scattering on sea surface and dynamic geometry of coastal global navigation satellite system-reflectometry, the altimetry performance is strongly dependent on elevation angle. As the elevation angle decreases, the bias in retrieved height using the peak of the derivative waveform and the fractional power point of the waveform leading edge increases. In this article, a multiparameter estimator is proposed to combine the peak of the derivative waveform and several fractional power points to obtain unbiased height. The simulated results show that the bias of the uncalibrated height using the proposed algorithm has no significant dependence on elevation angle, but the standard derivation for the low elevation angle case still is larger than that of the high elevation angle. In addition, the calibrated performance depends on the used fractional values so that proper fractional values should be chosen. The data from the Dongying experiment acquiring GPS L1 CA and L5 signal and the Qingdao experiment for BeiDou B1I signal are used to demonstrate the proposed algorithm. After calibrating using the proposed algorithm, regardless of GPS L1 CA, L5, or BeiDou B1I signal, the calibrated heights all are in agreement with *in situ* heights. Finally, the calibrated heights from the BeiDou B1I signal are used to retrieve sea surface height. The results show that retrieved sea surface heights from geostationary Earth orbit (GEO) and inclined geosynchronous orbit/middle Earth orbit (IGSO/MEO) satellites all appear in the same trend as that of the *in situ* ones; furthermore, GEO satellites can provide a better retrieved performance than IGSO/MEO satellites. Through averaging the heights from several satellites and smoothing with the half-hour span, compared to *in situ* sea surface height, the standard derivation of 0.67 m is obtained.**

***Index Terms*—Coastal altimetry, fractional point, global navigation satellite system-reflectometry (GNSS-R), multiparameter estimator, peak of derivative waveform, sea surface height.**

Manuscript received September 14, 2021; revised October 23, 2021; accepted November 19, 2021. Date of publication November 23, 2021; date of current version December 9, 2021. This work was supported in part by the National Natural Science Foundation of China under Grant 42104031 and Grant 31971781 and in part by the China Postdoctoral Innovative Talent Support Program under Grant BX20200039. *(Corresponding author: Lei Yang.)*

Feng Wang, Zhichao Xu, Dongkai Yang, GuoDong Zhang, Jin Xing, Zhejia Shi, and Bo Zhang are with the School of Electronic and Information Engineering, Beihang University, Beijing 100191, China (e-mail: wangf.19@163.com; by1602112@buaa.edu.cn; yangdongkai@sina.com; guodongzhang_q@163.com; 916941919@qq.com; szj14789@163.com; bozhang@buaa.edu.cn).

Lei Yang is with the School of Information Science and Engineering, Shandong Agricultural University, Shandong 271018, China (e-mail: yanglei_sdau@163.com).

Digital Object Identifier 10.1109/JSTARS.2021.3130050

I. Introduction

A LARGE number of the world's population lives in coastal regions and is very likely to be influenced by sea environment; therefore, it is important to detect and measure oceanic surges to monitor marine disaster and marine climate, such as storm surges and tsunamis in real time [1], [2]. The traditional way to measure sea level is tide gauges which require a supporting structure close to sea surface so that it is expensive to install and maintain [3]. In addition, the geodetic receiver should be needed for tide gauges to calibrate the vertical motion of the land. With the development of remote sensing, altimeter was proposed to observe sea surface height through transmitting electromagnetic wave to sea surface and measuring the propagation time of electromagnetic wave in space [4], [5]. Due to low spatial and temporal resolution, altimeters are difficult to work in the coastal region [6], [7]. Further, the altimeter not only needs a receiver but also has a high-power and high-cost transmitter so that it is unsuitable to be installed in coastal region.

In 1988, Hall and Cordey proposed the use of reflected global navigation satellite system (GNSS) signals from the sea surface to detect sea state [8]. Subsequently, in 1993, the concept of the passive reflectometry and interferometry system was proposed by Martin-Neira to improve the spatial and temporal sampling of mesoscale ocean altimetry [9]. This technology has been known as GNSS-reflectometry (GNSS-R) which uses the reflected GNSS signals from the Earth's surface to monitor Earth's physical parameters. During the last decades, it has been demonstrated that GNSS-R is capable of retrieving wind speed [10], [11], significant wave height [12], [13], sea surface height [14], [15], sea ice [16], [17], etc., for ocean application, and soil moisture [18], [19], vegetation [20], [21], etc., for land application. The detailed illustration on GNSS reflectometry and its application could be found in [22] and [23].

Sea surface height could be measured through estimating the delay between reflected and direct GNSS signals. At present, three GNSS reflectometry modes have been proposed to measure sea surface height. The first mode is the so-called interferometric GNSS-R (iGNSS-R) which cross-correlates the reflected GNSS signal with a direct one and could provide high altimetry performance due to the use of the encrypted GNSS signals; however, high-gain right handed circularly polarized (RHCP) and left handed circularly polarized (LHCP) antenna should be used to separate the signals from different satellites [24], [25]. Although

iGNSS-R uses the directive antenna, as the altitude decreases, the risk of cross-talk from undesired satellites increases [26]. The second is to use oscillating signal-to-noise ratio (SNR), carrier, and code phase outputted by positioning receiver [27], [28]. This technique is named as GNSS-interference/multipath reflectometry (GNSS-I/MR), which could provide centimeter-level altimetry precision. Geodetic antenna and receiver are designed to reduce multipath signals so that only GNSS signals from the low elevation angle satellites are used to measure sea surface height; therefore, this approach based on geodetic antenna and receiver has low temporal resolution [29]. A 10-year comparison of water levels measured using a geodetic GPS receiver versus tide gauge was carried out, and the results showed that the daily sampling number of individual estimations from GPS is from 20 to 40, and the corresponding sampling rate is from 0.6 to 1.2 h [30]. To use the signals over a greater range of satellite elevation angles, multiple low-cost antennas were used to measure water level in [29]. The results found that using a larger range of elevation angle can eliminate the gaps in time for daily tidal variation; however, the measurements were generally less precise at elevation angles greater than 30° because of lower RHCP components in signals. In addition, it should be noted that due to the extremely weak correlation between the chips of pseudo-random noise (PRN) code [31], when the path delay between the direct and reflected signal is over one chip length, the interference effect between the direct and reflected signal disappears so that GNSS-I/MR fails to work; therefore, GNSS-I/MR only works in low-height scenario, especially for high-rate code, such as GPS L5 and BeiDou B3I signal. The third approach is conventional GNSS-R which respectively tracks the code or carrier phase of the direct and reflected GNSS signals. Compared to the code, the carrier can provide the more precise estimation; however, the carrier can only be used in coherent scattering scenario [32], [33]. Code-based method has no such limitation and is widely used in ground-based, airborne, and spaceborne platforms. For the code-based method, it is more difficult to estimate the arrival time of the reflected GNSS signal than that of the direct GNSS signal. The usual approach to estimate the arrival time of the reflected signal is to track the positions of the feature points in the waveform, such as the peak of the derivative waveform (DER) [15] and the fractional-power point (HALF) [34]. Unfortunately, these estimations relative to the specular delay are biased due to the complex scattering on sea surface. It is known from the "Rayleigh criterion" [35] that diffuse scattering is significantly sensitive to the elevation angle; therefore, the biases between the estimated and specular delay are dependent on the elevation angle. For different elevation angles, DER biases for spaceborne GNSS-R altimetry range from ∼16.8 to 26.7 m for GPS C/A (coarse acquisition) code signal and from ∼6.1 to 9.4 m for Galileo E1 and BeiDou B1 OS signal [36]. Elevation-dependent precision for airborne and coastal GNSS-R ocean altimetry has been found in experiments [37] and [38]. In the experiment of [39], it was found that the elevation angle influence for coastal GNSS-R altimetry was about 4 m in coastal GNSS-R altimetry. The bias in retrieved height should be corrected to obtain high altimetry precision. In [40], the elevation angle influence on coastal code-based altimetry is investigated, and an approach was proposed to calibrate the elevation angle influence.

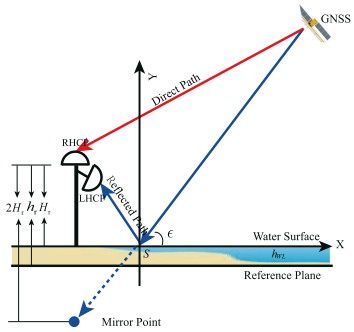

Fig. 1. Geometry of dual-antennal GNSS reflectometry.

This article focuses on coastal code-based GNSS-R altimetry to propose a new algorithm to obtain unbiased sea surface height. This method first retrieves sea surface height using the several defined retracker points and then to correct the bias through combining several retrieved sea surface heights from different retrackers using least square. Section II describes GNSS-R geometry and the frequently used feature points in the waveform and explains the bias in retrieved height. Section III presents the proposed algorithm to obtain unbiased sea surface height. In Sections IV and V, the simulation and experiment are conducted to demonstrate the proposed algorithm. Finally, Sections VI and VII address the discussion and conclusion of this article.

II. Coastal GNSS-R Altimetry

A. Geometry Model

The sea surface height is defined as

$$\mathrm{SSH} = h_{\mathrm{r}} - H_{\mathrm{r}} \tag{1}$$

where h_{r} is the receiver height relative to reference surface and H_{r} is the receiver height relative to sea surface. As given in Fig. 1, GNSS-R geometry is a trigonometry which is composed of the GNSS satellite, specular point, and receiver. For coastal scenario, the distances from GNSS satellite to specular point and receiver are far larger than that from receiver to specular point; therefore, the specular delay between direct and reflected signal is expressed as $\tau_{\mathrm{spec}} = 2H_{\mathrm{r}} \sin\theta / c$. When considering the vertical distance between RHCP and LHCP antenna, the receiver height relative to sea surface is derived as

$$H_{\mathrm{r}} = \frac{c\tau_{\mathrm{spec}} \sin\theta - d}{2} \tag{2}$$

where c is the propagation velocity of the electromagnetic wave; θ is the elevation angle of GNSS satellite; τ_{spec} is the specular delay between direct and reflected signal; d is the vertical distance between RHCP and LHCP antenna. h_{r} and d can be obtained from the precise measurement when the receiver is installed. θ is obtained through demodulating direct signal. It is important to precisely estimate the specular delay between direct and reflected signal to derive precisely receiver height relative to sea surface.

B. Specular Delay Estimation

Specular delay is derived through taking away the arrival time of the specular-reflected signal from the arrival time of the direct signal. The arrival time of the direct signal can be estimated using delay locked loop (DLL) [31]. Due to diffuse scattering, it is difficult to track the arrival time of the reflected signal through DLL. The usual approach is to retrack the location of the feature point in waveform. The feature points should be easy to extract from the waveform and is rarely influenced by other factors, such as noise and sea state. At present, two feature points have been used to estimate the delay between direct and reflected signal. DER retracker defines the feature point at the peak of the first derivative of the waveform as

$$\tau_{\mathrm{spec}} = \arg\max_{\tau} \left\{ \frac{dW_{\mathrm{N}}(\tau)}{d\tau} \right\} \tag{3}$$

where W_{N} is the normalized waveform of the reflected signal by its peak. With a complete model, the delay estimated using DER retracker is expressed as [15]

$$\hat{\tau}_{\mathrm{spec}} = \tau_{\mathrm{spec}} + \delta\tau_{\mathrm{spec}} \tag{4}$$

where $\delta\tau_{\mathrm{spec}}$ is a correction term. For an idealized situation in which the delay waveform can be represented by a convolution model, this correlation term appears when considering a band-limited receiver and a finite sampling rate [15]. However, in actual scenario which should include the complexly scattering mechanism between the electromagnetic wave on rough sea surface, space-dependent antenna pattern, the convolution model only is a simplification. In [40] and [41], it was found that this correction term is impacted on the elevation angle, receiver height, PRN code length, and wind speed.

The other retracker is HALF which is a threshold retracking algorithm taking the delay at a given fraction in the leading edge of the delay waveform as

$$W_{\mathrm{N}}(\tau_{\mathrm{spec}}) - \eta = 0 \tag{5}$$

where η is the given fractional value. The HALF retracker is derived from the threshold retracking of the traditional altimeter. In [42], a threshold retracking algorithm for ice-sheet height was presented, and the results showed that the threshold retracking algorithm with a 10% threshold level provided a more repeatable height estimation than other retracking algorithms. For GNSS-R, the point on the leading edge of the delay waveform at 70% of the peak has been chosen as the retracked point [34], [43]. A positive error caused by the arbitrary retracking point was presented in [34]. An 8.8-m calibrated bias is compensated for the retracking delay using 70% fractional point in [43]. These results indicate that similar to DER retracker, the delay estimated using HALF retracker also contains a bias. It should be noted that the results in [34] and [43] were respectively obtained from the airborne and spaceborne scenarios. A third-order polynomial is used to best fit the leading edge of the measured waveform to estimate the position of the defined retracker in waveform [44]. The position of DER retracker in the waveform is estimated using the second derivative of the fitted polynomial as

$$\tau_{\mathrm{DER}} = -\frac{A_2}{3A_3} \tag{6}$$

where A_2 and A_3 are the fitted coefficients for the quadratic and cubic terms of the three-order polynomial. HALF retracker is estimated through solving cubic equation $y(\tau) - \eta = 0$ (where $y(\tau)$ is the best fitted three-order polynomial) using Newton's method.

C. Height Bias

Here, to explain the bias in the retrieved height using DER and HALF retracker in the coastal scenario, the simulation is conducted. An usual model of the delay waveform is derived from the Kirchhoff approximation in a geometric optics limit and expressed as [45]

$$P(\tau) = \frac{P_t G_t \lambda^2}{(4\pi)^3} \times \int \frac{G_r(\boldsymbol{\rho})\,\Lambda^2(\tau - \tau(\boldsymbol{\rho}))\,\mathrm{sinc}^2(f_0 - f(\boldsymbol{\rho}))}{R_t^2(\boldsymbol{\rho})\,R_r^2(\boldsymbol{\rho})} \sigma_{pq}^2 d\boldsymbol{\rho} \tag{7}$$

where P_t and G_t are transmitted signal power and transmitting antenna gain; G_r is receiver antenna gain; λ is GNSS signal wavelength length; R_t and R_r are the distance from receiver and GNSS satellite to observation area; σ_{pq} is scattering coefficient; $\Lambda(\tau)$ is the correlation function between the PRN in reflected signal and the local replica. For a binary spreading sequence, when two are identical, $\Lambda(\tau)$ is defined as

$$\Lambda(\tau) = \begin{cases} 1 - \frac{|\tau|}{\tau_c} & |\tau| < \tau_c \\ 0 & |\tau| \geq \tau_c \end{cases} \tag{8}$$

where τ_c is the chip length. It should be noted that the model in (7) would have an incorrect result for the case of weak diffuse scattering or in the presence of coherent reflection [46]. Coherent reflections have been found from low-height scenario [47] so that the above equation may be imprecise to model the delay waveform; however, the objective of the simulation is only to explain the bias in retrieved height using DER and HALF retracker. Therefore, here, the above equation is still used instead of a more precise model of the delay waveform.

Fig. 2 shows the retrieved heights using DER and HALF retracker of 0.70 versus elevation angle when ground truth is 100 m. From the figure, it is seen that as the elevation angle increases, regardless of DER or HALF retracker, the retrieved heights contain negative biases which would result in a positive error in the measured sea surface height. Compared to HALF retracker of 0.70, DER retracker has a lower bias. Due to wider bandwidth, the retrieved height using L5 signal has far lower bias than that using L1 CA signal. The retrieved heights using DER and HALF retracker are expressed as

$$H_{\mathrm{r}} = H_{\mathrm{geo}} + \Delta H_{\mathrm{r}} \tag{9}$$

where H_{geo} is the ground-truth height; ΔH_{r} is the height bias.

Fig. 3 gives the changing relationships between the biases in retrieving height using DER and HALF retracker, in which whatever the fractional value η in (5) is, the biases from HALF

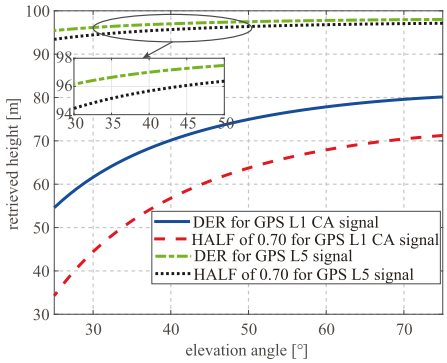

Fig. 2. Retrieved height using DER and HALF of 0.7 from simulated delay waveform versus elevation angle for GPS L1 CA and L5 signal when the ground truth is 100 m and the wind speed is 5 m/s for simulation scenario.

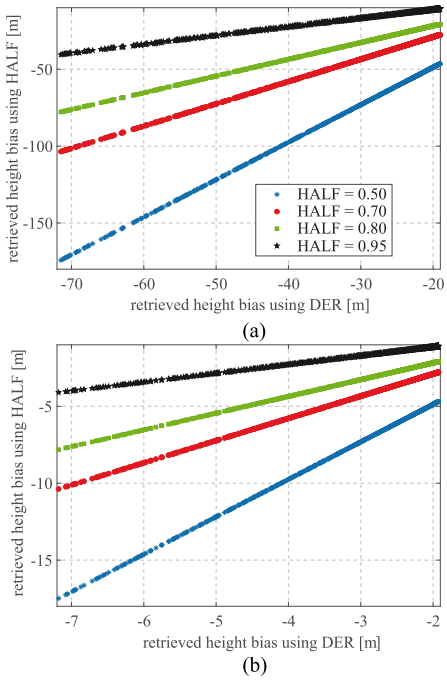

Fig. 3. Relationships between retrieved height biases using DER and ones using HALFs of 0.50, 0.70, 0.80, and 0.95, respectively, (a) for GPS L1 CA and (b) L5 signal. The noise-free delay waveforms used here are simulated using (7) when receiver height is 100 m, wind speeds is 5 m/s, and elevation angles are 25°–75° for simulation scenario.

retracker all appear to have linear relationships with the biases from DER retracker as

$$\Delta H_{\mathrm{rHALF}} = a \cdot \Delta H_{\mathrm{rDER}} + b \tag{10}$$

where $\Delta H_{\mathrm{rHALF}}$ and ΔH_{rDER}, respectively, are the biases in retrieved heights using HALF and DER retracker; a and b are linear coefficients.

III. Multiparameter Bias Calibration Algorithm

When combining DER retracker and several HALF retrackers with different fractional values, the equations can be expressed as

$$\begin{pmatrix} H_{\mathrm{rDER}} \\ H_{\mathrm{rHALF1}} - b_1 \\ \vdots \\ H_{\mathrm{rHALF}n} - b_n \end{pmatrix} = H_{\mathrm{geo}} \begin{pmatrix} 1 \\ 1 \\ \vdots \\ 1 \end{pmatrix} + \Delta H_{\mathrm{rDER}} \begin{pmatrix} 1 \\ a_1 \\ \vdots \\ a_n \end{pmatrix} \tag{11}$$

where $\Delta H_{\mathrm{rHALF}i}$ is the retrieved height using the ith defined HALF retracker; a_i and b_i are the linear coefficients of the relationship between the biases of DER and the ith HALF retracker. The above equation is expressed in the matrix form as

$$\mathbf{A} \cdot \mathbf{X} = \mathbf{Y} \tag{12}$$

where $\mathbf{A}$, $\mathbf{X}$, and $\mathbf{Y}$ are respectively

$$\mathbf{A} = \begin{pmatrix} 1 & 1 \\ 1 & a_1 \\ 1 & a_2 \\ \vdots & \\ 1 & a_n \end{pmatrix} \tag{13}$$

$$\mathbf{X} = \begin{pmatrix} H_{\mathrm{geo}} \\ \Delta H_{\mathrm{rDER}} \end{pmatrix} \tag{14}$$

$$\mathbf{Y} = \begin{pmatrix} H_{\mathrm{rDER}} \\ H_{\mathrm{r1}} - b_1 \\ H_{\mathrm{r2}} - b_2 \\ \vdots \\ \Delta H_{rn} - b_n \end{pmatrix}. \tag{15}$$

When a_i and b_i are determined beforehand, $\mathbf{A}$ is known and $\mathbf{Y}$ can be derived from the retrieved heights using DER and HALF retrackers. Unknown $\mathbf{X}$ is solved through least square as

$$\mathbf{X} = \left(\mathbf{A} \cdot \mathbf{A}^{\mathrm{T}}\right)^{-1} \mathbf{A}^{\mathrm{T}} \cdot \mathbf{Y}. \tag{16}$$

The first item in $\mathbf{X}$ is the unbiased height which is finally required for the measurement of sea surface height. Assuming that the measurements of different retrackers are independent and the errors are subject to the normal distribution, the mean and variance of the ith measurement error are $\langle e_{y_i} \rangle = 0$ and $V(e_{y_i}) = \sigma_y^2$, respectively. The covariance matrix of $\mathbf{X}$ is derived as

$$\begin{aligned} V(\mathbf{X}) &= \left\langle \left(\mathbf{A}^{\mathrm{T}}\mathbf{A}\right)^{-1} \mathbf{A}^{\mathrm{T}} \mathbf{e}_y \left(\left(\mathbf{A}^{\mathrm{T}}\mathbf{A}\right)^{-1} \mathbf{A}^{\mathrm{T}} \mathbf{e}_y \right)^{\mathrm{T}} \right\rangle \\ &= \left(\mathbf{A}^{\mathrm{T}}\mathbf{A}\right)^{-1} \mathbf{K}_y = \left(\mathbf{A}^{\mathrm{T}}\mathbf{A}\right)^{-1} \sigma_y^2 \end{aligned} \tag{17}$$

where $\mathbf{K}_y$ is the covariance matrix of $\mathbf{Y}$ and is expressed as $\mathbf{I}\sigma_y^2$. The variance of measured height H_{geo} is $\Pi \cdot \sigma_y^2$. Π is expressed as

$$\Pi = \frac{1 + \sum_{i=1}^{n} a_i^2}{(n+1)\left(1 + \sum_{i=1}^{n} a_i^2\right) - \left(1 + \sum_{i=1}^{n} a_i\right)^2}. \tag{18}$$

It is seen that the final precision of the retrieved height not only is determined by the measured error but also is impacted by the matrix $\mathbf{A}$. When chosen η for multiparameter observation

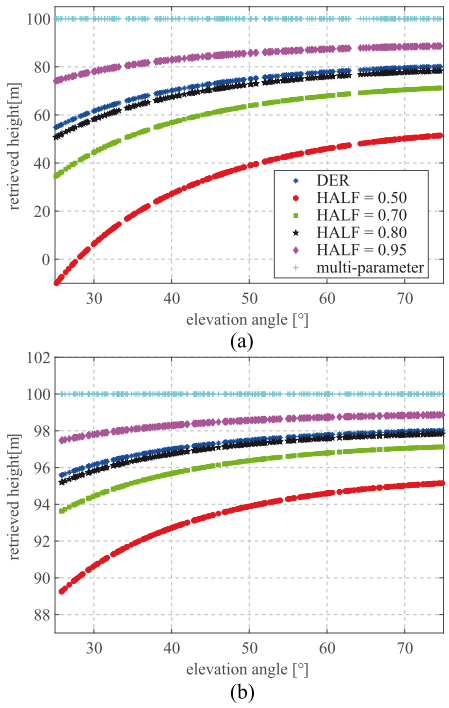

Fig. 4. Retrieved height using DER and HALFs, and calibrated height using multiparameter estimator for (a) GPS L1 CA and (b) L5 signal. The used delay waveforms are the same as Fig. 3.

has same or similar linear coefficient a_i, height variance tends to infinity. In other words, $\mathbf{A}$ is under rank and (16) is an underdetermined equation which has innumerable solutions. Hence, it is important to construct proper matrix $\mathbf{A}$ through choosing η to make Π to be low as far as possible.

Here, the availability of the proposed method is demonstrated using the noise-free delay waveform generated using model (7) when sea surface height and wind speed are, respectively, assumed as 0 m and 5 m/s, and elevation angles are respectively from 2 to 25 m/s and from 25° to 75°. Fig. 4 gives the comparison between uncalibrated and calibrated heights for different elevation angles. Compared to uncalibrated heights, the calibrated heights using the proposed algorithm are located at 100 m which is the ground truth and have no significant dependence on elevation angle. This indicates that the proposed algorithm is capable of correcting height bias.

Through simulating for different wind speeds, it is found that the matrix $\mathbf{A}$ is different; therefore, a lookup table (LUT) $\mathbf{A}$ parameterized as a function of the wind speed seems convenient.

IV. Simulation Demonstration

The simulation was conducted to evaluate the performance of the proposed algorithm. The simulation scenario is given in Table I, in which the receiver height relative to the reference surface is 100 m, and the sea surface height is set as the random number ranging from –1.5 to 1.5 m. Wind speed ranges from 2 to 25 m/s which covers a larger number of the coastal wind speed, and the elevation angle changes from 25° to 75°. Reflected signals not only contain additive white noise but also are distorted

TABLE I
Simulation Scenario Parameters

parameter	unit	value
receiver antenna height	m	100
elevation angle	°	$25 \sim 75$
sea surface height	m	$-1.5 \sim 1.5$
wind speed	m/s	$2 \sim 25$
incoherently averaged number	$\sim$	20000

by the multiplicative fading or speckle noise which is caused by the diffuse scattering from rough surface [48]. To model the delay waveform polluted by additive and multiplicative noise, the complex delay waveform of the reflected signal is modeled as [52]

$$Y_{si}(\tau) = \sqrt{\frac{P(\tau)}{2}} Z_{\mathrm{s}i} + \sqrt{P_n} \cdot Z_{\mathrm{n}i} \tag{19}$$

where Z_{si} and $Z_{\mathrm{n}i}$ are complex Gaussian white noise with real and imaginary parts, respectively; P_n is the noise power which is expressed as [49]

$$P_n = T_{\mathrm{c}}^2 k T_{\mathrm{R}} B_{\mathrm{w}} \tag{20}$$

where T_{c} is coherent integration time; k is the Boltzmann constant; T_{R} is the receiver noise equivalent temperature; B_{w} is the receiver bandwidth. To obtain the waveform with different SNRs, here, noise power is multiplied by a factor ξ as $P_n = \xi T_{\mathrm{c}}^2 k T_{\mathrm{R}} B_{\mathrm{w}}$. The above complex correlation waveforms are incoherently averaged as

$$\left\langle |Y_s(\tau)|^2 \right\rangle = \frac{1}{N} \sum_{i=1}^{N} Y_{\mathrm{s}i}(\tau) \cdot Y_{\mathrm{s}i}^*(\tau) \tag{21}$$

where N is the incoherent averaging number which is fixed as 20 000 here. It should be noted that the better performance can be obtained to take more independent waveform to incoherently average [44].

The detailed Monte Carlo simulation is as follows.

1) A group of elevation angles, sea surface heights, and wind speeds are randomly generated.
2) The above groups of parameters are used as the input to simulate the noise-free delay waveforms using (7).
3) The white noise and speckle noise are added into each noise-free delay waveform using (19) to generate 20 000 independent complex waveforms.
4) 20 000 independent complex waveforms are incoherently averaged using (21) to obtain noisy waveforms for each group.
5) The DER retracker and HALF retracker of 0.50, 0.75, 0.80, and 0.95 are used to estimate the delay and the heights are retrieved using (2) for each group.
6) The calibrated heights are obtained through (16).

Fig. 5(a) presents the scatter between the retrieved sea surface height using DER retracker and HALF retracker of 0.70 for the first case, in which the retrieved sea surface heights have clear biases with ground truth and are strongly dispersed. As given in Tables II and III , for L1 CA signal, the biases of the heights retrieved using DER retracker and HALF retracker of 0.7 with *in situ* ground truth are, respectively, −26.76 and

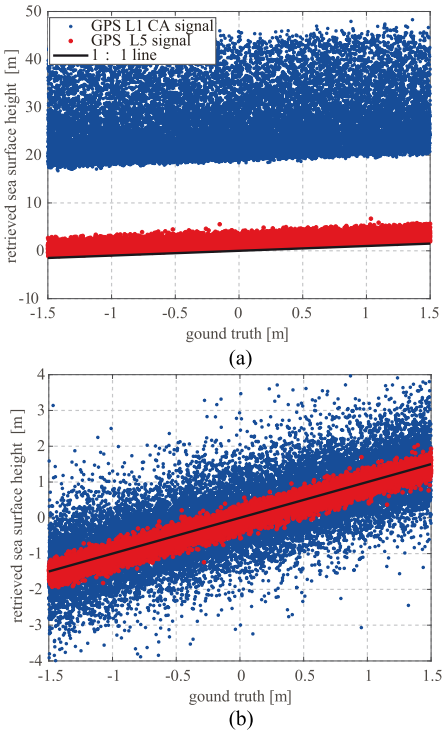

Fig. 5. (a) Retrieved height using DER retracker, and (b) calibrated height using multiparameter estimator for GPS L1 CA and L5 signal for the first case.

TABLE II
BIASES BETWEEN RETRIEVED SEA SURFACE HEIGHT USING DER, HALF, AND MULTIPARAMETER ESTIMATOR AND GROUND TRUTH (UNIT: M)

	DER	HALF				multi-parameter
		0.50	0.70	0.80	0.95	
L1 CA	-26.76	-64.97	-38.89	-29.03	-14.53	-0.02
L5	-1.69	-4.79	-2.36	-1.27	-0.55	0.02

TABLE III
STANDARD DERIVATIONS (σ_h) OF BETWEEN RETRIEVED SEA SURFACE HEIGHT USING DER, HALF, AND MULTIPARAMETER ESTIMATOR AND GROUND TRUTH (UNIT: M)

	DER	HALF				multi-parameter
		0.50	0.70	0.80	0.95	
L1 CA	6.78	16.22	9.74	7.26	3.61	0.79
L5	0.79	1.34	0.77	0.59	0.48	0.16

−38.89 m, and the corresponding standard derivations are 6.78 and 9.74 m. L5 signal provides the better performance, and the bias and standard derivation are both 10 times lower than that of L1 CA signal; however, the retrieved result still is unacceptable for coastal altimetry. In Fig. 4(b), which shows the comparisons of the sea surface heights calibrated through combining DER retracker and four HALF retrackers using (16) with ground truth, calibrated heights are in agreement with ground truth, and as given in Table II, the biases for L1 CA and L5 signal are both reduced to near 0. The standard derivations of L1 CA and L5 signal also decrease to 0.79 and 0.16 m, respectively. For coastal altimetry, after calibration using the proposed algorithm, the L5 signal obtains the formal precision and accuracy.

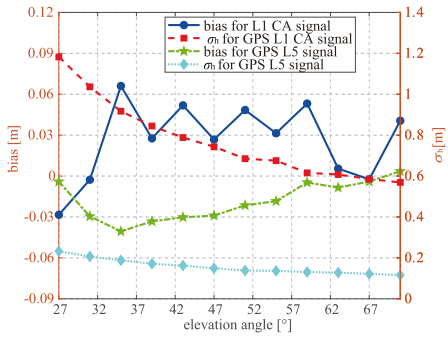

Fig. 6. Bias and standard derivation between retrieved sea surface height and ground truth versus elevation angle for GPS L1 CA and L5 signal.

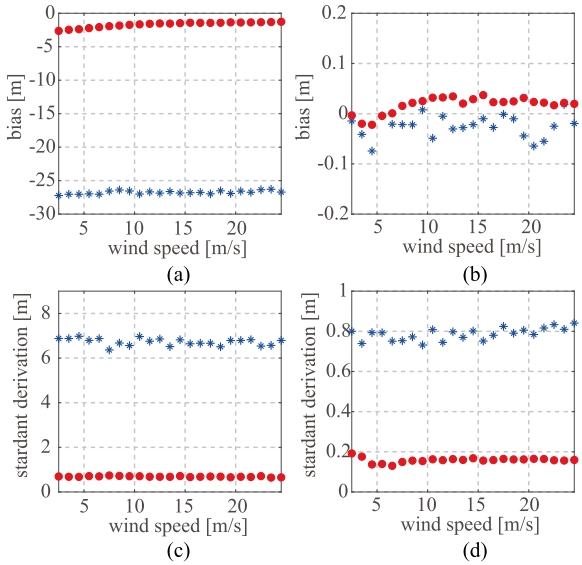

Fig. 7. (a), (b) Bias and (c), (d) standard derivation between retrieved sea surface height and ground truth versus wind speed for GPS L1 CA and L5 signal. (a) and (c) are the results using DER retracker. (b) and (d) are the results after the calibration. The red dot and the blue asterisk are respectively for GPS L5 signal L1 CA signal.

As shown in Fig. 2, the height biases from DER and HALF retracker seriously depend on elevation angle. Here, the dependencies of the biases and standard derivations of calibrated height on elevation angle are explored. Fig. 6 gives the changing trends of the biases and standard derivations after the calibration using the proposed algorithm. As elevation angle increases, the biases of the calibrated heights have no significant dependence on elevation angle, but standard derivations appear in a downward trend as elevation angle increases. This indicates that the proposed method can significantly calibrate the elevation-dependent bias in retrieved height; however, it is unable to weaken the dependence of the standard derivation on the elevation angle.

Wind speed or sea state has an impact on the tracking effect of DER and HALF retracker. Fig. 13(a) and (b), respectively, give the biases and standard derivations between retrieved sea surface height using DER retracker and ground truth, in which the absolute bias decreases as wind speed increases and gradually becomes stable after 15 m/s; however, the standard derivation appears weak depending on wind speed. After the calibration

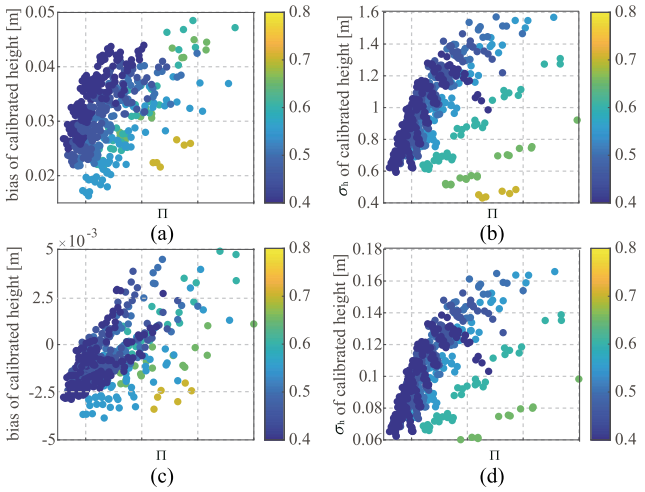

Fig. 8. (a), (c) Bias and (b), (d) standard derivation between calibrated sea surface height and ground truth versus Π for (a), (b) GPS L1 CA and (c), (d) L5 signal when the DER retracker and four HALF retrackers are combined to calibrate the height bias.

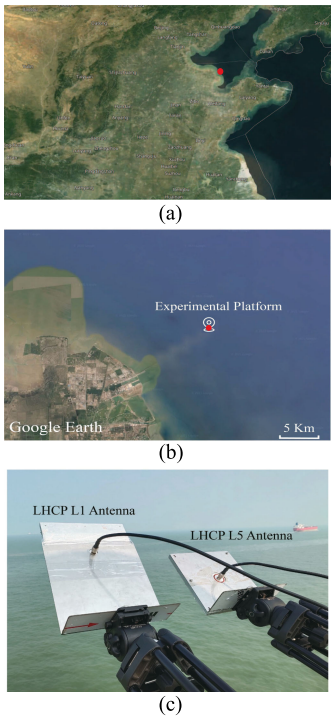

Fig. 9. (a) Aerial image (Google Earth) and (b) antenna setup of the Dongying GPS experiment.

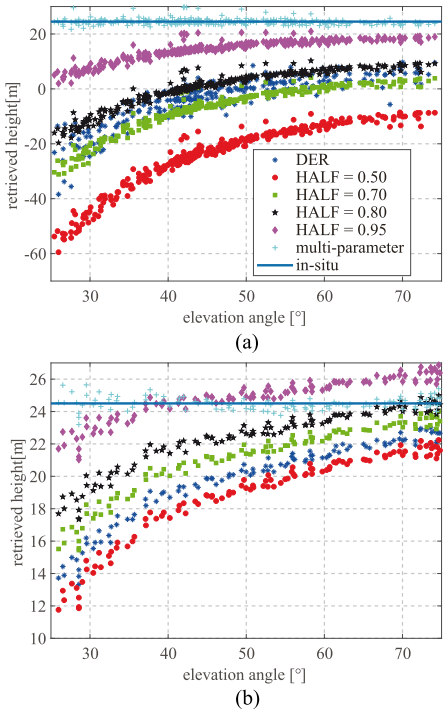

Fig. 10. Retrieved receiver height relative to sea surface versus elevation angle for (b) GPS L1 CA and (b) L5 signal in the Dongying experiment.

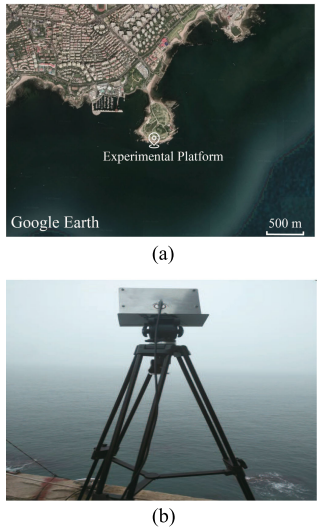

Fig. 11. (a) Aerial image (Google Earth) and (b) antenna setup of the Qingdao BeiDou experiment.

using the proposed algorithm, the bias and standard derivation both decrease and have no significant dependence on wind speed. This indicates that the proposed algorithm can reduce the measurement of sea surface height on wind speed. The wind speed is needed to know before calibrating sea surface height using the proposed algorithm. Coastal GNSS-R is capable of measuring wind speed or sea state [11], [50]; therefore, it is possible to calibrate the wind-dependent and elevation-dependent bias only using GNSS-R.

Π has an important influence on the calibration performance of the proposed algorithm. Fig. 8 shows the relationship between the calibration performance and Π, in which the biases and standard derivations of the uncalibrated heights appear to have positive proportional relationships with Π. In addition, it is seen that fractional value η also impact calibration performance. Better results can be obtained when the lower boundary of the used fractional values is lower. These results indicate that to obtain optimal calibration, it is important to choose a series of proper fractional values. The choosing procedure of the fractional

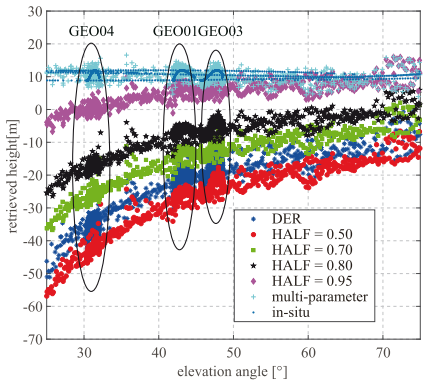

Fig. 12. Retrieved receiver height relative to sea surface versus elevation angle for the BeiDou B1I signal in the Qingdong experiment.

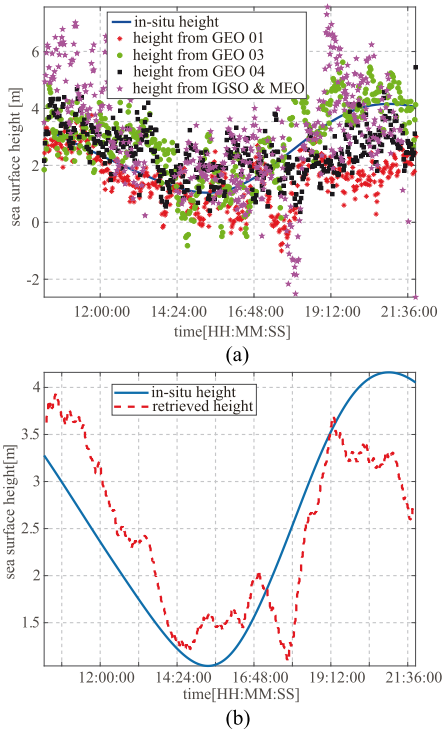

Fig. 13. Retrieved and *in situ* sea surface height of the Qingdao BeiDou experiment.

values can be considered as the optimization of the calibrated biases and standard derivations so that some optimization methods, such as gradient descent and genetic algorithm, can be used. This work goes outside the scope of this article; therefore, the optimal fractional values are not given here. In the following experimental demonstration, fractional values are fixed as 0.95, 0.80, 0.70, and 0.50.

V. Experiments

The actually acquired data from two experiments are used to demonstrate the significance of the proposed calibration algorithm. The first experiment was conducted to acquire the GPS L1 CA and L5 signals, and the second experiment was conducted to collect the BeiDou B1I signal.

A. Dongying GPS Experiment

The experiment was conducted at a wharf (38.154N, 119.066E) in Dongying of Shandong province in China from October 28 to November 2, 2020. To successfully collect the GPS L5 signal, the experiment time of every day is from 12:00 to 16:00. In this duration, the GPS PRN 24 satellite that transmits the L5 signal is visible for both RHCP and LHCP antennas. In addition, according to the *in situ* sea surface height provided by near tide gauge, the experiment site is microtidal environment, the tide difference in each day is about 60 cm, and sea surface height has weak variation of less than 10 cm during the acquiring period. The aerial image of the experimental site is shown in Fig. 9(a) and (b) from Google Earth, in which the red points mark the experiment site location. The experimental platform is located at Bohai Sea and far about 8.6 km away from the coast. There are no obstacles around the experimental site, which effectively avoids receiving multipath signals from rocks and small islands. Therefore, compared with the coast, the platform is more suitable for the coastal GNSS-R ocean altimetry experiment.

An RHCP L1/L5 GPS antenna in the zenith direction is used to receive direct signals. As illustrated in Fig. 10(b), an LHCP L1 GPS antenna and an LHCP L5 GPS antenna tilted with an azimuth angle of 65° and an elevation angle of 45° toward sea surface are used to receive the reflected signals. The antennas are installed on the wharf with an approximate height of 24.5 m above the sea surface.

In experiment, an acquisition device which consists of four-channel radio-frequency front end was used. The intermediate frequency (IF) of the device is 15.55 MHz. The IF analog signal is sampled and quantified with the sampling frequency of 62 MHz and the quantification number of 8 b. A software was developed to process the acquired data of GPS L1 CA and L5 signals. The software consists of direct and reflected channels to respectively process direct and reflected signals. The direct signals are tracked using closed-loop phase locked loop and DLL to provide the reference for the processing of reflected signal, and reflected signals are cross-correlated with a set of local replica signals with different delay to obtain the complex delay waveform. The parallel cross-correlation in frequency domain using fast Fourier transform (FFT) and inverse FFT is implemented. The coherent integration time in software is the same as the period of PRN code and both are 1 ms for L1 CA and L5 signals. After cross-correlation, a series of complex correlation values are incoherently averaged to obtain final delay waveform. DER retracker and the HALF retracker with the η of 0.95, 0.80, 0.70, and 0.50 are used to estimate the delay between direct and reflected signals.

Fig. 10 gives the changing trend of uncalibrated and calibrated heights versus elevation angle. From the results, similar to the simulation, uncalibrated heights show the strong dependence on elevation angle. In case of the lower elevation angle, the biases in retrieved height are larger. After calibration using multiparameter estimator, this dependence is greatly weakened, and calibrated heights are in agreement with the *in situ* height for both L1 CA and L5 signals. The corresponding biases and

TABLE IV
BIASES BETWEEN RETRIEVED RECEIVER HEIGHT USING DER, HALF, AND MULTIPARAMETER ESTIMATOR AND *IN SITU* HEIGHT IN THE DONGYING EXPERIMENT (UNIT: M)

	DER	HALF				multi-parameter
		0.50	0.70	0.80	0.95	
L1 CA	-28.02	-48.96	-31.82	-23.93	-10.29	0
L5	-4.64	-5.72	-3.38	-2.12	-0.36	0

TABLE V
STANDARD DERIVATION BETWEEN RETRIEVED RECEIVER HEIGHT USING DER, HALF, AND MULTIPARAMETER ESTIMATOR AND *IN SITU* HEIGHT IN THE DONGYING EXPERIMENT (UNIT: M)

	DER	HALF				multi-parameter
		0.50	0.70	0.80	0.95	
L1 CA	8.51	11.73	8.35	6.66	3.85	1.21
L5	2.53	2.81	2.23	1.91	1.30	0.40

standard derivations before and after calibration are given in Tables IV and V. Compared with uncalibrated heights, the biases of calibrated heights for both L1 CA and L5 signals almost reduce to 0, and the standard derivations respectively reduce to 1.21 and 0.40 m for L1 CA and L5 signals. These results indicate that the proposed algorithm is able to significantly correct the dependent bias of elevation angle to improve the measured performance. It is clear that the dispersion at low elevation angle is larger than that at high elevation angle, which is consistent with the phenomenon of decreasing standard derivation with increasing elevation angle in Fig. 6. It should be noted that it is difficult to obtain LUT of $\mathbf{A}$ parameterized as a function of the wind speed from limited experiment measurements; therefore, the matrix $\mathbf{A}$ is identical for different wind speed. This may be the reason that the calibrated sea surface heights still have weak fluctuation compared to *in-situ* data as shown in Fig. 10.

B. Qingdao BeiDou Experiment

As shown in Fig. 11(a) which is from Google Earth, the BeiDou experiment was conducted at a marine environmental monitoring station (36.059N, 120.437E) located on a small island in Qingdao, Shandong province of China. The experiment duration is from 10:15 to 21:51 on August 3, 2018. During the experiment, a falling tide from morning to afternoon and a rising tide from afternoon to evening were observed. The *in situ* sea surface heights were from near tide gauge. From *in situ* tide, it is found that the experiment region is mid-tidal environment with the tide difference being above 2 m.

An RHCP BeiDou antenna in the zenith direction is used to receive direct signals. As illustrated in Fig. 11(b), an LHCP BeiDou antenna tilted with an azimuth angle of 155° and an elevation angle of 45° toward sea surface are used to receive reflected signals. Except for the signals from MEO satellites, the signals from geostationary earth orbit (GEO) PRN01, PRN03, and PRN04 are also received by the RHCP and LHCP antennas. The antennas are installed on the wharf with an approximate height of 13 m above sea surface.

The used device synchronously acquiring direct and reflected BeiDou B1I signal was a two-channel digital collector with the IF of 3.996 MHz, the sampling frequency of 16.369 MHz, and the quantization number of 2 b. The used software is similar to the one described in Section VI-A, and the only difference is the generator of local replica signal.

TABLE VI
BIASES AND STANDARD DERIVATIONS BETWEEN RETRIEVED RECEIVER HEIGHT USING DER, HALF, AND MULTIPARAMETER ESTIMATOR AND *IN SITU* HEIGHT IN THE QINGDAO EXPERIMENT (UNIT: M)

	DER	HALF				multi-parameter
		0.50	0.70	0.80	0.95	
bias	-34.41	-11.73	-26.99	-19.88	-5.81	0
σ_{h}	8.55	9.64	7.21	5.94	3.47	1.58

TABLE VII
BIASES AND STANDARD DERIVATIONS BETWEEN RETRIEVED SEA SURFACE HEIGHT USING MULTIPARAMETER ESTIMATOR AND *IN SITU* SEA SURFACE HEIGHT IN THE QINGDAO EXPERIMENT (UNIT: M)

	GEO01	GEO03	GEO04	IGSO & MEO
bias	-0.95	0.38	-0.02	0.57
σ_{h}	0.98	0.77	1.03	1.50

Fig. 12 gives the comparison between uncalibrated and calibrated heights for the BeiDou B1I signal. Similar to the simulation and experimental results of GPS L1 CA and L5 signals, uncalibrated heights have monotonous dependent relationships with elevation angle, and the heights retrieved using the signals from inclined geosynchronous orbit/middle Earth orbit (IGSO/MEO) and GEO satellites appear to have the same dependence. This indicates that the heights from IGSO/MEO and GEO satellites can use the same linear coefficients to construct matrices $\mathbf{A}$ and $\mathbf{Y}$. Calibrated heights change about 13 m, which is the truth. The biases and standard derivations of uncalibrated and calibrated heights are given in Table VI which shows that compared to the height before calibration, calibrated height has further better results with the biases of near 0 and the standard derivation of 1.58 m.

Calibrated heights are used to retrieve sea surface height through (1). Fig. 13(a) gives retrieved sea surface heights from GEO PRN01, PRN03, PRN04, and IGSO/MEO satellites. The retrieved sea surface heights from both GEO and IGSO/MEO satellites have the same trend with *in situ* sea surface heights provided by near tide gauge. The corresponding biases and standard derivations are presented in Table VII. From the results, it is seen that the GEO satellite provides better results than IGSO/MEO satellites. The reason may be that for coastal altimetry, GEO satellites could provide relatively stable observation geometry.

With the falling and rising of the tide, as illustrated by the *in situ* data in Fig. 13(b), sea surface height slowly and smoothly varies. Here, retrieved sea surface heights from different satellites are combined to obtain formal sea surface heights. The first step is to average the retrieved heights from synchronously visible satellites at each observed time; and then averaged heights are smoothed with the half-hour span. The red line in Fig. 13 shows the finally retrieved sea surface height which clearly experiences a trend from fall to rise tide. The bias and standard derivation between retrieved and *in situ* sea surface height are –0.01 and 0.67 m, respectively. In some cases, because the differences of the measurement accuracies from different satellites are not considered, simply averaging the measurements from

several satellites may not obtain good performance. Weighted average could provide better results than the average; however, it requires that the measurements from different satellites have stable statistical characteristics. Due to the dynamic geometry, the statistical characteristics of the measurements from MEO satellites are unstable, and the visibility is time-varying. The GEO satellite can provide stable geometry so that the statistical characteristics are steady. Here, the measurements from GEO 01, 03, and 04 satellites are weightily averaged. The weighted values are computed from the standard derivations in Table VII as

$$w_i = \frac{1/\sigma_{\mathrm{h}i}^2}{\sum_{i=1}^{3} 1/\sigma_{\mathrm{h}i}^2} \tag{22}$$

where $\sigma_{\mathrm{h}i}$ is the standard derivation of the measurement from the $i\mathrm{th}$ GEO satellite. After the weighted average, the bias and standard derivation are, respectively, –0.08 and 0.54 m.

VI. Discussion

The evaluation indexes of the altimetry are bias and precision. The bias and standard derivation of the retrieved sea surface height through retracking DER and HALF in the waveform are strongly dependent on the elevation angle. As known, the motion of the GNSS satellite results in the variation of the elevation angle. Compared to MEO satellites, GEO satellites are stationary relative to Earth's surface and can provide stable geometry for coastal altimetry. Stable geometry makes the biases in retrieved heights using DER and HALF retracker to be relatively changeless. These fixed biases are easy to correct as systematic errors. In fact, there have been some works to focus on the altimetry based on GEO satellites, such as BeiDou GEO satellite [51], communication satellite [52], and digital video broadcasting satellite [53].

Wind speed is an influential impact on the measurement of sea surface height. The lower the wind speed is, the larger the bias of sea surface height using DER retracker is. Although the proposed algorithm can significantly calibrate this dependent bias, an LUT as a function wind speed should be developed beforehand so that it is necessary to acquire wind speed around the measurement region. It is attractive that the delay bias can be calibrated for the case of unknown wind speed. It is known that the specular points of several satellites are visible for a down-looking antenna. For coastal case, wind speed is identical in the coverage of the down-looking antenna. When assuming that the impact of wind speed for the measurement from different satellites are same, as presented in [41], it is possible to calibrate bias or improve the measurement performance through combining the measurements from several satellites [54], [55]. In some cases, due to the existing unreliable measurements, the fusion of several measurements may not obtain good performance but may pull down the performance. It is desirable to cross-check the consistence of all measurements to generate the consensus set and then fuse [56].

At present, sea surface height is measured using (1) and (2), which are geometric and analytical. Unlike traditional nadir-looking altimeters, GNSS-R has time-varying bistatic geometry so that it has more complex scattering mechanism and more influence factors. The analysis in this article found that the retrieved sea surface height contains a bias which depends on the elevation angle and wind speed. The antenna pattern also disturbs the delay waveform so that the azimuth angle may impact the measurement of sea surface height. The smaller reflectivity of wave crests than troughs also results in a bias called the electromagnetic bias in altimeter. The electromagnetic bias in GNSS-R has been analyzed in [57], and the results showed that the electromagnetic bias is dependent on the elevation angle, wind speed, and wind direction. In addition, the troposphere also introduces an additional delay in the reflected signal, especially for high-altitude and low-elevation case. This phenomenon has been used to sound the water vapor in troposphere [58]. In [59], a bias in the estimated height was found, that is elevation and height dependent, and can reach order of 1 m for a 90-m site. It is believed that the sea surface height could be seen as a multivariate nonlinear function of the estimated delay, elevation angle, azimuth angle, and wind speed, as $\mathrm{SSH} = f(\widehat{\tau}_{\mathrm{spec}}, \theta, \varphi, u_{\mathrm{ws}})$. Obviously, it is difficult to develop an accurate analytical expression to model the above relationship. Artificial intelligence (AI) which is advantageous to fit a complexly nonlinear relationship has been widely applied in the observation of the Earth's parameters [60], and, more recently, it also has been used in GNSS-R, such as retrieving wind speed [61]. It is valuable to train an AI model to accurately measure sea surface height. However, unlike the analytical method, AI model is data-driven so that a large number of measurements and *in situ* data are needed, and it undoubtedly increases the cost of developing the measurement model of sea surface height.

For GPS L1 CA and BeiDou B1I signals, even if the biases are corrected, due to low precision, retrieved heights still are unacceptable for altimetry application. Compared to L1 CA and BeiDou B1I signals, the GPS L5 signal provides the better performance because of the wider signal bandwidth. It has been demonstrated that signal bandwidth and incoherently averaging number of independent waveform have more important influence than SNR [52]. The use of wider bandwidth signal is an effective way to improve altimetry precision. In [62], the full broadcast spectrum consisting of multiple digital channels was processed as a single wideband signal to measure sea surface height, and centimeter-level precision was obtained. Some new signals, such as BOC modulation signal, have been transmitted by GNSS satellites. As known, Galileo E5 signal and BeiDou B2 signals adopt AltBOC(15, 10) modulation which modulates four codes onto two orthogonal subcarriers and occupies a wide bandwidth of around 51 MHz [63]. Except that Galileo E5a and E5b signals are individually used, it is possible to use the aggregate E5 signal through combining E5a and E5Q signals as a wideband signal [64], [65]. It is worth to believe that the use of the full-spectrum E5 and B2 signals would be able to obtain a better altimetry performance.

VII. Conclusion

The heights measured using DER and HALF retracker consist of the bias that depends on the elevation angle. This bias results

in an unacceptable measurement for coastal altimetry. This article proposed an algorithm to correct this bias using several retrackers in the leading edge of the waveform. The simulated results showed that compared to uncalibrated heights, the proposed calibration algorithm is able to significantly improve the performance of the retrieved height. After calibration, the biases have almost no dependence on elevation angle; however, the standard derivations decrease as the elevation angle increases. Compared to uncalibrated heights, the standard derivations of the calibrated height are 10 times lower for both GPS L1 CA and L5 signals. In addition, it was found that chosen fractional values in leading edge have an important impact on calibrated performance. Optimization methods can be used to find proper fractional values. The data from two experiments were used to demonstrate the proposed algorithm. Regardless of GPS L1 CA, L5, or BeiDou B1I signals, calibrated heights using the proposed algorithm all were in agreement with *in situ* heights. For the BeiDou B1I signal, through averaging the heights measured from several satellites and smoothing with the half-hour span, compared to *in situ* sea surface height, the bias of –0.01 m and the standard derivation of 0.67 m were obtained. Due to the weak fluctuation of sea surface height during the Dongying experiment, this article did not use GPS L1 CA and L5 signals to retrieve sea surface height; however, it still can be seen that because of the wider signal bandwidth, the L5 signal is capable of providing a better performance than L1 CA and BeiDou B1I signals. In future, the experiment will be conducted to test and evaluate the performance of coastal altimetry using the wider signal bandwidth, such as BeiDou B2 and Galieo E5 signals.

ACKNOWLEDGMENT

The authors would like to thank Wei Liu, Yongqing Yu, Linfeng Wang, Xiang Dong, Haining Wang, and Pengfei Zhu for providing access to local tide gauge data and helping with the coastal altimetry experiment.

REFERENCES

[1] B. Neumann *et al.*, "Future coastal population growth and exposure to sea-level rise and coastal flooding - A global assessment," *Plos One*, vol. 10, no. 3, 2015, Art. no. e0131375.

[2] P. L. Vu *et al.*, "Identifying 2010 Xynthia storm signature in GNSS-R-based tide records," *Remote Sens.*, vol. 11, pp. 1–16, 2019.

[3] F. Romano *et al.*, "Tsunami source of the 2021 M_W 8.1 Raoul Island earthquake from DART and tide-gauge data inversion," *Geophys. Res. Lett.*, vol. 48, 2021, Art. no. e2021GL094449.

[4] G. D. Quartly *et al.*, "Retrieving sea level and freeboard in the Arctic: A review of current radar altimetry methodologies and future perspectives," *Remote Sens.*, vol. 11, no. 7, p. 881, 2019.

[5] X. Dong and C. Huang, "Monitoring global mean sea level variation with TOPEX/Poseidon altimetry," *Acta Geod. Cartogr. Sin.*, vol. 29, pp. 266–272, 2000.

[6] J. Bouffard, S. Vignudelli, P. Cipollini, and Y. Menard, "Exploiting the potential of an improved multimission altimetric data set over the coastal ocean," *Geophys. Res. Lett.*, vol. 35, no. 21, 2008, Art. no. L10601.

[7] P. Cipollini *et al.*, "Monitoring sea level in the coastal zone with satellite altimetry and tide gauges," *Surv. Geophys.*, vol. 38, pp. 33–57, 2017.

[8] C. D. Hall and R. A. Cordey, "Multistatic scatterometry," in *Proc. IEEE Int. Geosci. Remote Sens. Symp.*, Edinburgh, U.K., 1988, pp. 561–652.

[9] M. Martin-Neria, "A passive reflectometry and interferometry system (PARIS): Application to ocean altimetry," *ESA J.*, vol. 17, pp. 331–355, 1993.

[10] W. Lin, M. Portabella, G. Foti, A. Stoffelen, C. Gommenginger, and Y. He, "Toward the generation of a wind geophysical model function for spaceborne GNSS-R," *IEEE Trans. Geosci. Remote Sens.*, vol. 57, no. 2, pp. 655–666, Feb. 2019.

[11] F. Wang, D. Yang, B. Zhang, W. Li, and J. Darrozes, "Wind speed retrieval using coastal ocean-scattered GNSS signals," *IEEE J. Sel. Topics Appl. Earth Observ. Remote Sens.*, vol. 9, no. 11, pp. 5272–5283, Nov. 2016.

[12] F. Soulat *et al.*, "Sea state monitoring using coastal GNSS-R," *Geophys. Res. Lett.*, vol. 31, no. 21, 2004, Art. no. L21303.

[13] A. Alonso-Arroyo *et al.*, "Retrieval of significant wave height and mean sea surface level using the GNSS-R interference pattern technique: Results from a three-month field campaign," *IEEE Trans. Geosci. Remote Sens.*, vol. 53, no. 6, pp. 3198–3209, Jun. 2015.

[14] S. Ozafrain, P. A. Roncagliolo, and C. H. Muravchik, "Likelihood map waveform tracking performance for GNSS-R ocean altimetry," *IEEE J. Sel. Topics Appl. Earth Observ. Remote Sens.*, vol. 12, no. 12, pp. 5379–5384, Dec. 2019.

[15] A. Rius, E. Cardellach, and M. Martin-Neira, "Altimetric analysis of the sea-surface GPS-reflected signals," *IEEE Trans. Geosci. Remote Sens.*, vol. 48, no. 4, pp. 2119–2127, Apr. 2010.

[16] Q. Yan and W. Huang, "Sea ice thickness measurement using spaceborne GNSS-R: First results with TechDemoSat-1 data," *IEEE J. Sel. Topics Appl. Earth Observ. Remote Sens.*, vol. 13, pp. 577–587, 2020.

[17] W. Li, E. Cardellach, F. Fabra, A. Rius, S. Rib, and M. Martn-Neira, "First spaceborne phase altimetry over sea ice using TechDemoSat-1 GNSS-R signals," *Geophys. Res. Lett.*, vol. 44, no. 16, pp. 8369–8376, Aug. 2017.

[18] C. Yin *et al.*, "Intercomparison of soil moisture retrieved from GNSS-R and from passive L-band radiometry at the Valencia Anchor Station," *Sensors*, vol. 19, pp. 1–16, 2019.

[19] J. F. Munozmartin *et al.*, "Soil moisture estimation synergy using GNSS-R and L-band microwave radiometry data from FSSCat/FMPL-2," *Remote Sens.*, vol. 13, p. 994, 2021.

[20] Q. Chen, D. Won, D. M. Akos, and E. E. Small, "Vegetation sensing using GPS interferometric reflectometry: Experimental results with a horizontally polarized antenna," *IEEE J. Sel. Topics Appl. Earth Observ. Remote Sens.*, vol. 9, no. 10, pp. 4771–4780, Oct. 2016.

[21] H. Carrenoluengo, G. Luzi, and M. Crosetto, "Above-ground biomass retrieval over tropical forests: A novel GNSS-R approach with CyGNSS," *Remote Sens.*, vol. 12, no. 9, p. 1368, 2020.

[22] V. U. Zavorotny, S. Gleason, E. Cardellach, and A. Camps, "Tutorial on remote sensing using GNSS bistatic radar of opportunity," *IEEE Geosci. Remote Sens. Mag.*, vol. 2, no. 4, pp. 8–45, Dec. 2014.

[23] S. Jin, E. Cardellach, and F. Xie, *GNSS Remote Sensing: Theory, Methods and Applications*. Dordrecht, The Netherlands: Springer, 2014.

[24] E. Cardellach *et al.*, "Consolidating the precision of interferometric GNSS-R ocean altimetry using airborne experimental data," *IEEE Trans. Geosci. Remote Sens.*, vol. 52, no. 8, pp. 4992–5004, Aug. 2014.

[25] A. Rius *et al.*, "Altimetry with GNSS-R interferometry: First proof of concept experiment," *GPS Solut.*, vol. 16, no. 2, pp. 231–241, 2012.

[26] R. Onrubia, D. Pascual, and H. Park, "Satellite cross-talk impact analysis in airborne interferometric global navigation satellite system-Reflectometry with the microwave interferometric reflectometer," *Remote Sens.*, vol. 11, no. 9, p. 1120, 2019.

[27] K. M. Larson, J. S. Lofgren, and R. Haas, "Coastal sea level measurements using a single geodetic GPS receiver," *Adv. Space Res.*, vol. 51, no. 8, pp. 1301–1310, 2013.

[28] S. Jin, X. Qian, and X. Wu, "Sea level change from BeiDou Navigation Satellite System-Reflectometry (BDS-R): First results and evaluation," *Glob. Planetray Change*, vol. 149, pp. 20–25, 2017.

[29] D. J. Purnell *et al.*, "Precise water level measurements using low-cost GNSS antenna arrays," *Earth Surf. Dynam.*, vol. 9, no. 3, pp. 673–685, 2021.

[30] K. M. Larson, R. D. Ray, and S. D. P.Williams, "A 10-year comparison of water levels measured with a geodetic GPS receiver versus a conventional tide gauge," *J. Atmos. Ocean. Technol.*, vol. 34, no. 2, pp. 295–307, 2017.

[31] E. D. Kaplan and C. J. Hegarty, *Understanding GPS Principles and Application*, 2nd ed. Norwood, MA, USA: Artech House, 2006, pp. 153–240.

[32] E. Cardellach *et al.*, "First precise spaceborne sea surface altimetry with GNSS reflected signals," *IEEE J. Sel. Topics Appl. Earth Observ. Remote Sens.*, vol. 13, pp. 102–112, 2020.

[33] W. Li, E. Cardellach, F. Fabra, S. Ribo, and A. Rius, "Lake level and surface topography measured with spaceborne GNSS-reflectometry from CYGNSS mission: Example for the Lake Qinghai," *Geophys. Res. Lett.*, vol. 45, no. 24, pp. 13332–13341, 2018.

[34] J. Mashburn, P. Axelrad, S. T. Lowe, and K. M. Larson, "An assessment of the precision and accuracy of altimetry retrievals for a Monterey Bay GNSS-R experiment," *IEEE J. Sel. Topics Appl. Earth Observ. Remote Sens.*, vol. 9, no. 10, pp. 4660–4668, Oct. 2016.
[35] P. Beckmann and A. Spizzichino, *The Scattering of Electromagnetic Waves From Rough Surfaces*. Norwood, MA, USA: Artech House, 1987.
[36] W. Li, E. Cardellach, F. Fabra, S. Rib, and A. Rius, "Assessment of spaceborne GNSS-R ocean altimetry performance using CYGNSS mission raw data," *IEEE Trans. Geosci. Remote Sens.*, vol. 58, no. 1, pp. 238–250, Jan. 2020.
[37] F. Fabra *et al.*, "Is accurate synoptic altimetry achievable by means of interferometric GNSS-R?," *Remote Sens.*, vol. 11, no. 5, p. 505, 2019.
[38] H. Carreno-Luengo, A. Camps, I. Ramos-Perez, and A. Rius, "Experimental evaluation of GNSS-reflectometry altimetric precision using the P(Y) and C/A signals," *IEEE J. Sel. Topics Appl. Earth Observ. Remote Sens.*, vol. 7, no. 5, pp. 1493–1500, May 2014.
[39] Y. Zhang *et al.*, "Study of accurate ocean-altimetry with GNSS-R," in *Proc. IEEE Int. Geosci. Remote Sens. Symp.*, 2013, pp. 1410–1413.
[40] G. Zhang *et al.*, "Evaluation and correction of elevation angle influence for coastal GNSS-R ocean altimetry," *Remote Sens.*, vol. 13, no. 15, p. 2978, 2021.
[41] F. Wang *et al.*, "Measurement of the sea surface height with airborne GNSS reflectometry and delay bias calibration," *Remote Sens.*, vol. 13, p. 3014, 2021.
[42] C. H. Davis, "A robust threshold retracking algorithm for measuring ice-sheet surface elevation change from satellite radar altimeters," *IEEE Trans. Geosci. Remote Sens.*, vol. 35, no. 4, pp. 976–979, Jul. 1997.
[43] J. Mashburn, P. Axelrad, S. T. Lowe, and K. M. Larson, "Global ocean altimetry with GNSS reflections from TechDemoSat-1," *IEEE Trans. Geosci. Remote Sens.*, vol. 56, no. 7, pp. 4088–4097, Jul. 2018.
[44] S. Ribo, J. C. Arco, S. Oliveras, E. Cardellach, A. Rius, and C. Buck, "Experimental results of an X-band PARIS receiver using digital satellite TV opportunity signals scattered on the sea surface," *IEEE Trans. Geosci. Remote Sens.*, vol. 52, no. 9, pp. 5704–5711, Sep. 2014.
[45] V. U. Zavorotny and A. G. Voronovich, "Scattering of GPS signals from the ocean with wind remote sensing application," *IEEE Trans. Geosci. Remote Sens.*, vol. 38, no. 2, pp. 951–964, Mar. 2000.
[46] A. G. Voronovich and V. U. Zavorotny, "Bistatic radar equation for signals of opportunity revisited," *IEEE Trans. Geosci. Remote Sens.*, vol. 56, no. 4, pp. 1959–1968, Apr. 2018.
[47] J. F. Munoz-Martin *et al.*, "Untangling the incoherent and coherent scattering components in GNSS-R and novel application," *Remote Sens.*, vol. 12, p. 1208, 2020.
[48] S. Gleason, C. Gommenginger, and D. Crowell, "Fading statistics and sensing accuracy of ocean scattered GNSS and alyimetry signals," *Adv. Space Res.*, vol. 46, no. 2, pp. 208–220, 2010.
[49] S. T. Gleason, "Remote sensing of ocean, ice and land surfaces using bistatically scattered GNSS signals from low Earth orbit," Ph.D. thesis, Univ. Surrey, Surrey, U.K., 2006.
[50] W. Li *et al.*, "Initial results of typhoon wind speed observation using coastal GNSS-R of BeiDou GEO satellite," *IEEE J. Sel. Topics Appl. Earth Observ. Remote Sens.*, vol. 9, no. 10, pp. 4720–4729, Oct. 2016.
[51] J. Wu *et al.*, "Sea surface estimation by ground-based BDS GEO satellite reflectometry," *IEEE J. Sel. Topics Appl. Earth Observ. Remote Sens.*, vol. 13, pp. 5550–5559, 2020.
[52] R. Shash, J. L. Garrison, and M. S. Grant, "Demonstration of bistatic radar for ocean remote sensing using communication satellite signals," *IEEE Geophys. Res. Lett.*, vol. 9, no. 4, pp. 619–623, Jul. 2012.
[53] R. Shah and J. L. Garrison, "Precision of Ku-band reflected signals of opportunity altimetry," *IEEE Geophys. Res. Lett.*, vol. 14, no. 10, pp. 1840–1844, Oct. 2017.
[54] X. An *et al.*, "Modelling global ionosphere based on multi-frequency, Multi-constellation GNSS observations and IRI model," *Remote Sens.* vol. 12, p. 439, 2020.
[55] F. Chen, L. Liu, and F. Guo, "Sea surface height estimation with Multi-GNSS and wavelet de-noising," *Sci. Rep.*, vol. 9, 2019, Art. no. 15181.
[56] S. K. Kim and J. Park, "Monitoring a storm surge during hurricane Harvey using multi-constellation GNSS-reflectometry," *GPS Solut.*, vol. 25, p. 63, 2021.
[57] A. Ghavidel, D. Schiavulli, and A. Camps, "Numberical computation of the electromagnetic bias in GNSS-R altimetry," *IEEE Trans. Geosci. Remote Sens.*, vol. 54, no. 1, pp. 489–498, Jan. 2016.
[58] M. J. Shafei and M. Mashhadi-Hossainali, "Application of the GNSS-R in tomographic sounding of the Earth atmosphere," *Adv. Space Res.*, vol. 62, pp. 71–83, 2018.
[59] S. D. P. Williams and F. G. Nievinski, "Tropospheric delays in ground-based GNSS multipath reflectometry-experimental evidence from coastal sites," *J. Geophys. Res. Solid Earth*, vol. 122, pp. 2310–2327, 2017.
[60] G. E. Manucharyan, L. Siegelman, and P. Klein, "A deep learning approach to spatiotemporal sea surface height interpolation and estimation of deep currents in geostrophic ocean turbulence," *J. Adv. Model. Earth Syst.*, vol. 13, 2021, Art. no. e2019MS001965.
[61] J. Reynolds, M. P. Clarizia, and E. Santi, "Wind speed estimation from CYGNSS using artificial neural networks," *IEEE J. Sel. Topics Appl. Earth Observ. Remote Sens.*, vol. 13, pp. 708–716, 2020.
[62] S. C. Ho *et al.*, "Wideband ocean altimetry using Ku-band and K-band satellite signals of opportunity: Proof of concept," *IEEE Geophys. Res. Lett.*, vol. 16, no. 7, pp. 1012–1016, Jul. 2019.
[63] N. C. Shivaramaiah and A. G. Dempster, "The Galileo E5 AltBOC: Understanding the signal structure," in *Proc. Int. Glob. Navig. Satell. Syst. Soc.*, Queensland, Australia, 2009, pp. 1–3.
[64] H. T. Diessongo *et al.*, "Exploiting the Galileo E5 wideband signal," *Inside GNSS*, pp. 64–73, 2012.
[65] H. Ma, M. Antoniou, and M. Cherniakov, "Passive GNSS-based SAR resolution improvement using joint Galileo E5 signals," *IEEE Geophys. Res. Lett.*, vol. 12, no. 8, pp. 1640–1644, Apr. 2015.

Feng Wang received the bachelor's degree in electronic information engineering from the School of Electronic and Information Engineering, Beihang University, Beijing, China, in 2012 and the master's degree in communication and information engineering and the Ph.D. degree in information and signal processing from the School of Electronic and Information Engineering, Beihang University, Beijing, China, in 2014 and 2019, respectively .

In 2020, he started his postdoctoral work with the School of Electronic and Information Engineering, Beihang University. His research interest includes global navigation satellite system reflectometry (GNSS-R) application in ocean observation.

Zhichao Xu received the bachelor's degree in electronic information engineering from the School of Electronic and Information Engineering, Shandong University, Shandong, China, in 2003 and the master's degree in geographic information engineering from Information Engineering University, Zhengzhou, China, in 2008. He is currently working toward the Ph.D. degree in information and signal processing from the School of Electronic and Information Engineering, Beihang University, Beijing, China.

His research interest includes global navigation satellite system reflectometry (GNSS-R) application in ocean observation.

Dongkai Yang was born in 1972, in China. He received the B.S. degree in electronic engineering from the North University of China, Taiyuan, China, in 1994, and the M.S. and Ph.D degrees in communication and information system from Beihang University, Beijing, China, in 1997 and 2000, respectively.

From 2001 to 2002, he was a Research Fellow with the Nanyang Technological University, Singapore. Since 2010, he has been a Full Professor with the School of Electronic and Information Engineering, Beihang University. His research interests include global navigation satellite system (GNSS) and its application.

GuoDong Zhang received the bachelor's degree from the School of Information Science and Engineering, Shandong University, Jinan, China, in 2015 and the master's degree in communication and information engineering from the School of Electronic and Information Engineering, Beihang University, Beijing, China, in 2017. He is currently working toward the Ph.D. degree in information and signal processing from the School of Electronic and Information Engineering, Beihang University, Beijing, China.

His research interests include global navigation satellite system reflectometry (GNSS-R) application in ocean observation.

Jin Xing received the bachelor's degree in electronic and information engineering from the School of Information Engineering, China University of Geosciences, Beijing, China, in 2016 and the master's degree in electronic and information engineering from Hainan University, Haikou, China, in 2019. He is currently working toward the Ph.D. degree in information and signal processing with Beihang University, Beijing, China.

His research interest includes global navigation satellite system reflectometry (GNSS-R) application in ocean observation.

Zhejia Shi received the bachelor's degree in measurement and control from Aerospace Engineering University, in 2016. He is currently working toward the master's degree in electronic and information engineering with Beihang University, Beijing, China.

His research interest includes global navigation satellite system reflectometry (GNSS-R) application in ocean observation.

Bo Zhang received the Ph.D. degree in communication and information system from the School of Electronic and Information Engineering, Beihang University, Beijing, China, in 2006.

From 2006 to 2009, he was a Postdoctoral Researcher of Electronic Science and Technology. Since 2009, he has been a Lecturer with the School of Electronic and Information Engineering, Beihang University. His research interests include GNSS and spread spectrum communication.

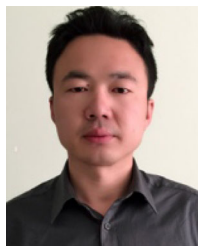

Lei Yang was born in 1983, in China. He received the B.S. and M.S. degrees in computer science from Northwest Polytechnical University, Xi'an, China, in 2004 and 2008, respectively, and the Ph.D. degree in agricultural electrification and automation from Shandong Agricultural University, Tai'an, China, in 2017.

Since 2012, he has been a Lecturer with the School of Information Science and Technology, Shandong Agricultural University. His current research interests include GNSS-R and ASIC design.